

In Situ Array Calibration for Synthetic Aperture Sonar

Jeremy Dillon and Shannon-Morgan Steele

Kraken Robotic Systems Inc.

Mount Pearl, NL, Canada

{jdillon, ssteele}@krakenrobotics.com

Abstract—The focusing of a synthetic aperture requires precise phase alignment of signals that are combined coherently to form an image. Synthetic aperture sonars are typically operated using multi-channel receiver arrays to maximize the achievable area coverage rate, which places strict requirements on calibration accuracy of the acoustic elements. Conventional sonar calibration is a time-consuming process requiring specialized facilities, and array calibration may change due to environmental conditions such as temperature and operating depth. In this paper, we describe an *in situ* calibration technique for an array installed in an autonomous underwater vehicle using backscatter from diffuse targets on the seabed as the calibration source. The technique includes compensation for vehicle motion and range-variant corrections for bistatic geometry and phase curvature of the received wavefield. Results are presented for a modular receiver array with an installation-induced phase error that caused image blurring and grating lobes. The calibration technique quantified the installation offset and restored the imagery to its properly focused state. A simulation of the sonar impulse response is also presented to confirm that the measured phase error was the root cause of the observed image artifacts.

Index Terms—synthetic aperture sonar, sonar imaging, calibration

I. INTRODUCTION

Synthetic Aperture Sonar (SAS) is a high-resolution technique for imaging the seabed with sound waves. The along-track motion of the sensor platform is used to synthesize an aperture with a length that increases with range, thereby achieving constant centimetric resolution in both the along-track and across-track directions. Since acoustic returns are combined coherently in SAS image formation, proper focusing of the aperture requires motion compensation with sub-wavelength accuracy and precise phase alignment from ping to ping. SAS achieves an extremely high Area Coverage Rate (ACR) by operating at lower frequency than conventional sidescan sonar to reduce acoustic absorption. As a result, SAS systems employ multi-channel receiver arrays to increase the allowable ping-to-ping displacement, eliminate range ambiguities, and maximize the achievable ACR [1]. The combination of multi-channel receiver arrays and strict requirements on phase accuracy implies that the array must be precisely calibrated to form high quality imagery.

Conventional sonar array calibration is a time-consuming process requiring specialized facilities such as a large test tank, precisely machined mounting brackets, an omni-directional



Fig. 1. AquaPix® Miniature Synthetic Aperture Sonar (MINSAS) with modular receiver array (four receiver modules and two transmitter modules shown), electronics pressure vessel (large cylinder), and port and starboard oil compensation units (small cylinders).

sound source, sound speed measurement, and accurately known relative positions between the source and receiver. Furthermore, calibration may change upon installation of the array in the host platform, or under the influence of operating conditions such as temperature and distortion that may occur due to pressure loads that vary with ocean depth. Fortunately, alternative calibration techniques exist for the case where the received wavefield is spatially correlated [2]. Amplitude calibration is a relatively straightforward process using channel equalization techniques. Phase calibration may be achieved by processing backscattered signals from point targets or diffuse scatterers, as described in the medical ultrasound literature [3]. For both scattering cases, the spatial correlation function of the scatterer distribution is well approximated by a delta function or impulse. Similar techniques have also been proposed for radar arrays [4] and real aperture sidescan sonar [5].

In this paper, we describe an *in situ* calibration technique for a SAS array installed in an Autonomous Underwater Vehicle (AUV). One of the challenges inherent in SAS array calibration is that the nonlinear component of the platform motion often greatly exceeds the acoustic wavelength. SAS systems are also operated in the near field of the array, which

induces a range-variant phase curvature that must be removed prior to calibration. The proposed technique only requires acoustic backscatter from a relatively flat featureless seabed. Corrections are made for platform motion as well as bistatic geometry and range-variant phase curvature so that the array can be calibrated while the vehicle operates under typical conditions (e.g., during a survey mission at ocean depth).

The array calibration technique is presented in Section II, beginning with a brief discussion of the effects of calibration errors on image quality. Motion compensation and range-variant corrections performed prior to phase calibration are also described. Results are presented in Section III for the AquaPix® MINSAS modular receiver array, which is shown in Figure 1. SAS imagery is presented for an AUV installation that included a mechanically induced phase error, which was estimated and corrected using the calibration technique. In Section IV, the validity of the phase error estimate is confirmed by simulating the MINSAS 2D impulse response while applying the experimentally measured phase error. The simulated along-track grating lobes are similar to those present in the distorted image. Conclusions are presented in Section V.

II. THEORY

Array calibration errors cause periodic amplitude or phase variation along the synthetic aperture, which result in image defocusing and grating lobes. The effects of many types of phase error are demonstrated in [6]. Grating lobes are secondary peaks in the SAS impulse response with an along-track spacing Δx given by

$$\Delta x = \frac{R\lambda}{2VT} \quad (1)$$

where R is the range to the target, λ is the acoustic wavelength, V is the vehicle speed, and T is the pulse repetition period. The term VT in the denominator represents the ping-to-ping displacement, which is also the spatial period of the aperture phase error. To ensure continuity of spatial sampling, the speed and pulse repetition period must satisfy

$$VT \leq \frac{L_R}{2} \quad (2)$$

where L_R is the length of the receiver array.

SAS arrays are often spatially sampled with an element spacing $d \geq \lambda/2$, which causes azimuthal ambiguities that must be suppressed with the transmitter and receiver beam-patterns [7]. The minimum spatial sampling rate, or Nyquist sampling rate, is $d = L_T$, where L_T is the effective length of the transmitter. Enhanced ambiguity suppression is obtained by oversampling the receiver array, for example, by placing the null of the receiver element beampattern in the first side-lobe of the transmitter beampattern with an element spacing $d = 2L_T/3$ as in [8], which is also the design approach taken for Kraken's MINSAS. The van Cittert–Zernike theorem then implies that adjacent receiver channels are partially correlated when backscatter is received from a diffuse target such as a flat featureless seabed [9]. Correlation between adjacent channels is exploited in Section II-D to obtain the phase calibration.

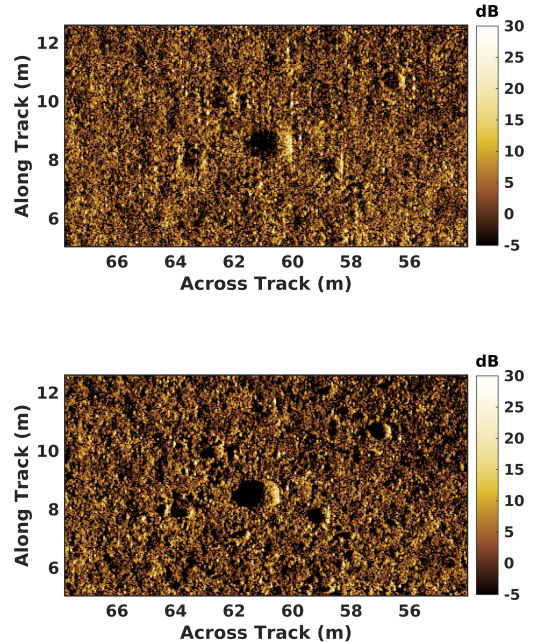


Fig. 2. MINSAS seabed image with installation-induced phase error (top) and corrected image after calibration (bottom).

A. Amplitude calibration

Amplitude calibration is obtained by equalizing the signal levels for each receiver channel. Let $z_{ij}(n)$ represent sample n in time of the complex acoustic signal from channel i and ping j after demodulation and matched filtering. The signal level in dB for channel i is given by

$$\text{dB}_i = 10 \log_{10} \left(\frac{1}{NP} \sum_{n=1}^N \sum_{j=1}^P |z_{ij}(n)|^2 \right) \quad (3)$$

where N is the number of range samples per ping and P is the number of pings. The average signal level for an array of M channels is

$$\overline{\text{dB}} = \frac{1}{M} \sum_{i=1}^M \text{dB}_i. \quad (4)$$

A gain of $\overline{\text{dB}} - \text{dB}_i$ is then applied to each channel for amplitude calibration.

B. Motion compensation

Although an AUV flies along a nominally straight trajectory, small angular motions cause time-varying phase shifts along the array which are removed prior to calibration. The relevant component of rotation is slant range yaw ψ_{sr} , which is the projection of the rotation vector in the direction normal to the slant range plane [10]. For each ping and each range bin, the slant range direction is measured using angle-of-arrival

interferometry [11]. The slant range angle β relative to a point on the seabed is given by

$$\beta = \phi + \arcsin\left(\frac{C\Delta t}{D}\right) \quad (5)$$

where ϕ is the roll angle of the array, C is the speed of sound, Δt is the observed time delay between two vertically separated rows of acoustic elements, and D is the interferometric baseline, i.e., the spacing between upper and lower rows. Time delay is estimated by cross-correlating upper and lower channels of the array [12]. Changes in vehicle yaw ψ and pitch θ are projected in the slant range direction via

$$\Delta\psi_{sr} = \Delta\psi \cos\beta + \Delta\theta \sin\beta. \quad (6)$$

Slant range yaw for each range bin is obtained by integrating (6) over the number of pings. A linear phase shift is applied along the array to compensate for slant range yaw.

C. Phase center approximation

During phase calibration, signals are averaged across a series of range bins to maximize the accuracy of the estimate from a given number of pings. The bistatic nature of the SAS array induces a range-variant phase curvature that is removed prior to calibration. The Phase Center Approximation (PCA) replaces the bistatic sonar geometry with an equivalent monostatic configuration by advancing the received signals in time [10], with a time offset τ_i given by

$$\tau_i = \frac{\Delta_i^2}{4RC} \quad (7)$$

where Δ_i is the bistatic baseline for channel i (i.e., the spatial separation between the transmitter and receiver element i). When (7) is applied to demodulated sonar data, a phase rotation of $2\pi f_0 \tau_i$ radians is also applied, where f_0 is the demodulation frequency.

The PCA time shift depends on range in two ways. In addition to the presence of R in the denominator, the bistatic baseline Δ_i varies with range because the receiver array is in motion during reception of the ping. Motion estimation performed during SAS micronavigation provides a precise measurement of vehicle speed and the component of sway in the slant range direction, so that Δ_i is a known function of range for each channel. The received signals for each ping are partitioned into a series of non-overlapping range bins, with (7) and the corresponding phase rotation applied to each bin.

D. Phase calibration

The first step of phase calibration is to correlate adjacent channels of the receiver array while averaging over the number of pings and the number of samples in each range bin:

$$\Delta\phi_{ik} = \angle\left(\sum_{n=1}^N \sum_{j=1}^P z_{ij}(n)z_{i+1,j}^*(n)\right) \quad (8)$$

where $\Delta\phi_{ik}$ is the angle of the complex correlation coefficient for range bin k and channels i and $i+1$, * denotes complex conjugation, and $z_{ij}(n)$ now represents acoustic data that

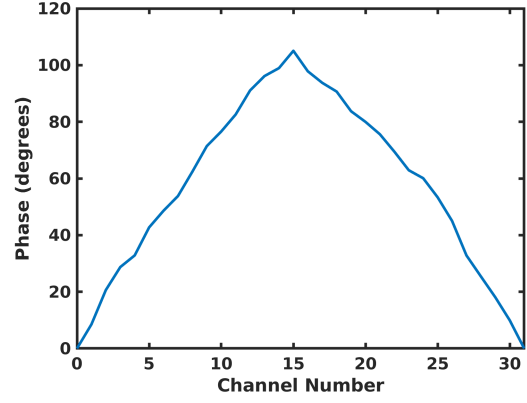


Fig. 3. Measured phase error along MINSAS port array. The aft and forward modules correspond to channel numbers 0–15 and 16–31, respectively.

has been demodulated, matched filtered, and compensated as described in Sections II-B and II-C. The spherical propagation of acoustic wavelets causes a range-dependent quadratic phase curvature that is removed with the correction

$$\widehat{\Delta\phi_{ik}} = \Delta\phi_{ik} - \frac{\pi d^2}{R_k \lambda} \left(i - \frac{M}{2}\right) \quad (9)$$

where R_k is the range of bin k . Finally, the array phase calibration coefficients are obtained by averaging over K range bins and integrating along the array:

$$\phi_{i+1} = \phi_i + \frac{1}{K} \sum_{k=1}^K \widehat{\Delta\phi_{ik}}. \quad (10)$$

III. RESULTS

Normally it is not necessary to calibrate individual MINSAS modules. The acoustic elements are matched to within a few degrees of phase, the module housings are machined from solid titanium blocks for the 6000 m depth-rated version, and the modules are attached to a rigid backing plate to ensure alignment between modules. The example presented in this paper is unique in that the modules were installed in an AUV with a carbon fiber frame with a small depression on the port side where the forward and aft modules meet. The depression was undetected at the time of installation.

The data for the top image of Figure 2 was collected from the port side of the AUV at a depth of approximately 3000 m. SAS beamforming focused the data to improve the resolution compared to the corresponding real aperture image. However, numerous grating lobes are evident. Individual point-like targets appear as multiple repeated copies in the along-track direction, which cause a loss of contrast in the shadow region behind the rocks. The fact that the starboard imagery was well focused ruled out vehicle motion as the cause of image degradation.

The amplitude calibration showed no significant differences between channels. However, the phase calibration shown in Figure 3 revealed an approximately linear phase error along

each module. In Figure 3, channel numbers 0–15 and 16–31 correspond to the aft and forward modules, respectively. The peak phase error at the center of the array represents a displacement of 1.3 mm toward the vehicle interior and an angular offset of 1.4° between modules.

In post-processing, the acoustic data was reprocessed using the phase calibration from Figure 3 to obtain the image in the lower panel of Figure 2. It is clear that the grating lobes have been removed and the shadow contrast is improved. It can also be seen that the phase error caused a fictitious across-track displacement during the SAS motion estimation process. Prior to a subsequent deployment of the AUV, the port side array was re-installed with a shim to correct the 1.3 mm displacement, which resulted in well focused imagery on port and starboard sides without calibration. Estimated calibration coefficients can also be applied during real-time SAS processing if it is not practical to correct the installation mechanically. Calibration would also be necessary if a module exhibited a nonlinear phase offset, such as a quadratic phase error, that cannot be removed with mechanical adjustment.

IV. SIMULATION

The MINSAS 2D impulse response was simulated by considering an ideal point target moving past the sonar. The simulation assumed a monostatic geometry and utilized the stop-and-hop approximation [13]. The relative azimuth angle between the sonar and target was computed for each transmit/receive position. The measured along-track transmit and receive beam patterns were applied to each ping. For simplicity, it was assumed that the target is centered in the vertical beam of the sonar. Range-dependent propagation loss was applied in the form of spherical spreading and acoustic absorption. At each along-track position of the synthetic aperture, the simulated signal was demodulated and matched filtered. The SAS impulse response was obtained by applying the backprojection image formation algorithm to the simulated acoustic data.

The effect of a module angular offset was demonstrated by considering a point target at the same location as the large rock in Figure 2, located at 8.5 m along-track and 61 m across-track. To simulate the array offset, the measured phase error from Figure 3 was applied in a periodic pattern along the synthetic aperture. The applied phase error causes grating lobes in the along-track direction, as shown in Figure 4. The across-track direction of the image is unaffected. The spacing of the grating lobes is approximately 0.25 m, consistent with (1) and the distorted SAS image in Figure 2.

V. CONCLUSION

In this paper, we have described a calibration technique for a SAS array installed on an AUV. Amplitude calibration is performed using channel equalization. Phase calibration is achieved by processing backscattered signals from diffuse scatterers. The proposed technique only requires acoustic backscatter from a relatively flat featureless seabed. Corrections are made for platform motion as well as bistatic geometry and range-variant phase curvature. The estimated

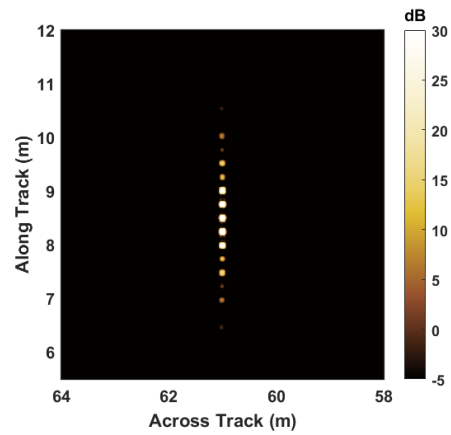


Fig. 4. Simulated 2D SAS impulse response of a MINSAS receiver array with modules installed with an angular offset caused by the phase error shown in Figure 3.

calibration coefficients may be applied during post-processing by reprocessing the raw acoustic data, or the coefficients can be applied on-the-fly by a real-time processor.

Calibration results were presented for the case where a MINSAS receiver array was installed with an angular offset between fore and aft modules, which resulted in image blurring and grating lobes. The array calibration technique identified the installation error and estimated the installation offset. A properly focused image was obtained by applying the calibration coefficients in post-processing. The correctness of the calibration technique was further confirmed when the installation was repeated with shims to remove the estimated offset, which resulted in well focused imagery without correction. The proposed technique is generally applicable to any SAS system with an oversampled receiver array and has the advantage of performing the calibration *in situ* under typical operating conditions.

REFERENCES

- [1] L. J. Cutrona, "Comparison of sonar system performance achievable using synthetic-aperture techniques with the performance achievable by more conventional means," *Journal of the Acoustical Society of America*, vol. 58, no. 2, pp. 336–348, 1975.
- [2] J. P. Hamaker, J. D. O'Sullivan, and J. E. Noordam, "Image sharpness, Fourier optics, and redundant-spacing interferometry," *Journal of the Optical Society of America*, vol. 67, no. 8, pp. 1122–1123, 1977.
- [3] S. W. Flax and M. O'Donnell, "Phase-aberration correction using signals from point reflectors and diffuse scatterers: Basic principles," *IEEE Transactions on Ultrasonics, Ferroelectrics and Frequency Control*, vol. 35, no. 6, pp. 758–767, 1988.
- [4] E. H. Attia and B. D. Steinberg, "Self-cohering large antenna arrays using the spatial correlation properties of radar clutter," *IEEE Transactions on Antennas and Propagation*, vol. 37, no. 1, pp. 30–38, 1989.
- [5] B. L. Douglas, H. Lee, and C. D. Loggins, "A calibration technique for sidescan sonar systems based on the second-order statistics of returned signals," *Proc. IEEE OCEANS, Newport, RI, USA*, 1992.
- [6] D. A. Cook and D. C. Brown, "Analysis of phase error effects on stripmap SAS," *IEEE Journal of Oceanic Engineering*, vol. 34, no. 3, pp. 250–261, 2009.
- [7] K. D. Rolt and H. Schmidt, "Azimuthal ambiguities in synthetic aperture sonar and synthetic aperture radar imagery," *IEEE Journal of Oceanic Engineering*, vol. 17, no. 1, pp. 73–79, 1992.

- [8] A. Bellettini and M. Pinto, "Design and experimental results of a 300–kHz synthetic aperture sonar optimized for shallow-water operations," *IEEE Journal of Oceanic Engineering*, vol. 34, no. 3, pp. 285–293, 2009.
- [9] R. Mallart and M. Fink, "The van Cittert–Zernike theorem in pulse echo measurements," *Journal of the Acoustical Society of America*, vol. 90, no. 5, pp. 2718–2727, 1991.
- [10] A. Bellettini and M. A. Pinto, "Theoretical accuracy of synthetic aperture sonar micronavigation using a displaced phase-center antenna," *IEEE Journal of Oceanic Engineering*, vol. 27, no. 4, pp. 780–789, 2002.
- [11] R. E. Hansen, T. O. Sæbø, K. Gade, and S. Chapman, "Signal processing for AUV based interferometric synthetic aperture sonar," *Proc. IEEE OCEANS, San Diego, CA, USA*, 2003.
- [12] A. H. Quazi, "An overview on the time delay estimate in active and passive systems for target localization," *IEEE Transactions on Acoustics, Speech, and Signal Processing*, vol. ASSP-29, no. 3, pp. 527–533, 1981.
- [13] M. A. Richards, *Fundamentals of Radar Signal Processing*. McGraw-Hill, 2005.